arXiv:0810.4822v1 [cond-mat.mes-hall] 27 Oct 2008

Coherent spin radiation by magnetic nanomolecules and nanoclusters

V.I. Yukalov[1], V.K. Henner[2,3], P.V. Kharebov[3], and E.P. Yukalova[4]

[1] *Bogolubov Laboratory of Theoretical Physics, Joint Institute for Nuclear Research, Dubna 141980, Russia*

[2] *University of Louisville, Louisville, Kentucky 40292, USA*

[3] *Perm State University, Perm 614000, Russia*

[4] *Laboratory of Information Technologies, Joint Institute for Nuclear Research, Dubna 141980, Russia*

Abstract

The peculiarities of coherent spin radiation by magnetic nanomolecules is investigated by means of numerical simulation. The consideration is based on a microscopic Hamiltonian taking into account realistic dipole interactions. Superradiance can be realized only when the molecular sample is coupled to a resonant electric circuit. The feedback mechanism allows for the achievement of a fast spin reversal time and large radiation intensity. The influence on the level of radiation, caused by sample shape and orientation, is analysed. The most powerful coherent radiation is found to occur for an elongated sample directed along the resonator magnetic field.

Key words: coherent radiation; radiowave sources; molecular magnets; relaxation effects; numerical simulation; magnetic anisotropy

PACS: 75.50.Xx, 75.30.Gw, 75.40.Gb, 75.40.Mg, 75.60.Es, 07.57.Hm

1 Nanomolecules and nanoclusters

The possibility of realizing coherent spin relaxation, in the regime of *collective induction*, was advanced by Bloembergen and Pound [1], who suggested to couple the spin sample to a resonant electric circuit. In the presence of a resonator, there can also arise five other regimes of coherent spin motion producing coherent radiation: *maser generation, pure superradiance, triggered superradiance, pulsing superradiance, and punctuated superradiance*, whose detailed description can be found in review articles [2,3]. At the first stage, coherent relaxation effects have been studied for nuclear spins [4–10]. Recently [11–14], the possibility of coherent spin relaxation in molecular magnets, possessing large electronic spins, was suggested.

Molecular magnets are composed of magnetic nanomolecules having several properties essentially distinguishing molecular spins from nuclear spins (see review articles [3,11,15,16]). First of all, magnetic molecules can possess different values of the total spin, including rather large spins. As examples we can mention the following molecules, whose spins are shown in brackets:

$$\mathrm{K_6\left[V_{15}^{4+}As_6\ O_{42}(H_2O)\right]\ 8H_2O} \qquad \left(\mathrm{S}=\frac{1}{2}\right)\ ,$$

$$\mathrm{(Ph\ Si\ O_2)_6Cu_6(O_2\ Si\ Ph)_6} \qquad (\mathrm{S}=3)\ ,$$

$$\mathrm{[Mn_{12}O_{12}(CH_3COO)_{16}(H_2O)_4]\,(2CH_3COOH)\ 4H_2O} \qquad (\mathrm{S}=10)\ ,$$

$$\mathrm{[Fe_8O_2(OH)_{12}T_6]^{8+}} \qquad (\mathrm{S}=10)\ ,$$

$$\mathrm{Mn_6O_4Br_4(Et_2\ dbm)_6} \qquad (\mathrm{S}=12)\ ,$$

$$\mathrm{[Cr(CN\ Mn\ L)_6]\,(Cl\ O_4)_9} \qquad \left(\mathrm{S}=\frac{27}{2}\right)\ .$$

The linear size of such molecules is about 1nm$=10\mathring{A}$. A system of these molecules forms a crystalline cluster with a well organized crystalline lattice, whose spacing is around $14\mathring{A}$. Below the blocking temperature of approximately 1K, each magnetic nanomolecule possesses, in its ground state, a total spin S, that is, the magnetic moment $\mu_B S$. The magnetization reversal is caused by the weak spin-phonon interactions, because of which the reversal process is extremely slow, lasting for $T_1 \sim 10^5 - 10^7$ s. More detailed information on magnetic nanomolecules can be found in Refs. [3,11,15,16].

In addition to magnetic nanomolecules, there exists a whole series of magnetic nanoclusters that also exhibit large total spins [11,17–19]. Such clusters can be formed by metals, e.g., Ni, Fe, Co, Hg, by oxides, NiO, Fe_2O_3 and like that, and by alloys, for instance, $NiFe_2O_4$, $Nd_2Fe_{14}B$, $Pr_2Fe_{14}B$, $Tb_2Fe_{14}B$, $DyFe_{14}B$, $Pr_2Co_{14}B$, $Sm_1Fe_{11}Ti_1$, $Sm_1Fe_{10}V_2$, $Sm_2Fe_{17}N_{23}$, $Sm_2Fe_{17}C_{22}$, Sm_2Co_{17}, and $SmCo_5$. These nanoclusters can be of various sizes, with diameters between $10\mathring{A}$ to $10^4\mathring{A}$. The total spin S can range between 10^2 to 10^4. So, the total magnetic moment can be very large. For illustration, we may give some parameters for iron-platinum nanoclusters [20-22]. Thus, the nanocluster compound $Fe_{50}Pt_{50}$ possesses an effective spin $S \sim 2\times 10^4$. The Curie temperature plays the role of the blocking temperature, for this material being $T_c = 710$ K. The uniaxial anisotropy parameter $D = K_c V_c$, with the anisotropy strength $K_c = 0.6 \times 10^8$ erg/cm^3. The typical diameter of $63\mathring{A} = 6.3$ nm corresponds to a spherical cluster of volume $V_c = 1.31\times 10^{-19}$ cm^3. So, the anisotropy parameter is $D = 0.785 \times 10^{-11}$ erg, and $D/\hbar = 0.745 \times 10^{16}$ s^{-1}. The escape time for temperatures below T_c is larger than 10^{32} s. The nanoclusters of $Fe_{70}Pt_{30}$ have effective spins $S \sim 2 \times 10^3$, Curie

temperature $T_c = 420$ K, and the cubic anisotropy strength $K_c = 0.8 \times 10^7$ egr/cm^3. With a typical diameter of $23\mathring{A} = 2.3$ nm, the volume of a spherical cluster is $V_c = 0.637 \times 10^{-20}$ cm^3. The corresponding anisotropy parameter $D = 0.51 \times 10^{-13}$ erg, and $D/\hbar = 0.483 \times 10^{14}$ s^{-1}. Escape times at low temperatures are extremely long.

The problem, we address in the present paper, is as follows. Suppose we consider a system of nanomolecules or nanoclusters. For short, we shall mention in what follows nanomolecules, keeping in mind that the same consideration is applicable to nanoclusters. Being placed in an external magnetic field, the system can be strongly spin polarized. Then, the system, magnetized in one direction, is placed in an external magnetic field of the opposite direction. That is the way of preparing a strongly nonequilibrium system. The natural process of magnetization reversal in such a system is extremely slow, being characterized by the time T_1. The reversal can be made essentially faster by applying strong transverse external fields, either static or alternating [3,19,23]. However, the fastest relaxation can be achieved by coupling the spin sample with a resonator [3,11–14], when the relaxation process becomes coherent.

The faster the relaxation process, the stronger the radiation intensity produced by moving spins. And the coherent spin relaxation results in coherent spin radiation. As has been mentioned above, there are several types of coherent spin radiation [2,3]. The fastest spin relaxation and, respectively, the strongest radiation intensity occurs, when the process is self-organized. Such a self-organized coherent radiation is called *superradiance*.

It is important to emphasize that the conditions of spin superradiance are very different from those of atomic superradiance [24,25] and acoustic superradiance [26]. In spin systems, because of the strong decoherence, caused by dipole interactions, superradiance is impossible without a resonator [3,11–14,27].

The aim of the present paper is to find the optimal conditions under which spin superradiance reaches the largest radiation intensity.

2 Equations of motion

The consideration is based on the microscopic Hamiltonian

$$\hat{H} = \sum_i \hat{H}_i \; + \; \frac{1}{2} \sum_{i \neq j} \hat{H}_{ij} \; , \tag{1}$$

in which $\hat{H}_i$ is a single-molecule term and $\hat{H}_{ij}$ describes molecular spin interactions. The single-particle term

$$\hat{H}_i = -\mu_0 \mathbf{B} \cdot \mathbf{S}_i - D(S_i^z)^2 \tag{2}$$

includes the Zeeman energy, with the electron magnetic moment $\mu_0 = -2\mu_B$, and the single-site magnetic axial anisotropy term, with the anisotropy parameter D. Generally, there can also be present a cubic anisotropy, with a term of the type $-D[(S_i^x)^2(S_i^y)^2 + (S_i^y)^2(S_i^z)^2 + (S_i^z)^2(S_i^x)^2]$. However, such terms are usually small. The magnetic field

$$\mathbf{B} = B_0 \mathbf{e}_z + H \mathbf{e}_x \tag{3}$$

contains an external static magnetic field B_0 and the resonator feedback field H. The interaction term

$$\hat{H}_{ij} = \sum_{\alpha\beta} D_{ij}^{\alpha\beta} \; S_i^\alpha \; S_j^\beta \tag{4}$$

is due to dipole interactions, with the dipolar tensor

$$D_{ij}^{\alpha\beta} = \frac{\mu_0^2}{r_{ij}^3}\left(\delta_{\alpha\beta} - 3n_{ij}^{\alpha}\, n_{ij}^{\beta}\right) , \tag{5}$$

where

$$r_{ij} \equiv |\mathbf{r}_{ij}| , \qquad \mathbf{n}_{ij} \equiv \frac{\mathbf{r}_{ij}}{r_{ij}} , \qquad \mathbf{r}_{ij} \equiv \mathbf{r}_i - \mathbf{r}_j .$$

The resonator is an electric circuit surrounding the spin sample [3]. The resonator feedback field is formed by a magnetic coil and is described by the Kirchhoff equation

$$\frac{dH}{dt} + 2\gamma H + \omega^2 \int_0^t H(t')\, dt' = -4\pi\eta\, \frac{dm_x}{dt} , \tag{6}$$

in which γ is the resonator damping, ω is the resonator natural frequency, η is a filling factor, and

$$m_x \equiv \frac{\mu_0}{V} \sum_j < S_j^x > \tag{7}$$

is the transverse magnetization density, V being the sample volume. Molecules are enumerated by the index $j = 1, 2, \ldots, N$, each molecule possessing spin S, with the spin vector $\mathbf{S}_i = \{S_i^{\alpha}\}$. In what follows, we set the filling factor $\eta = 1$.

The characteristic frequencies of the system are the Zeeman frequency

$$\omega_0 = -\frac{\mu_0}{\hbar}\, B_0 = \frac{2}{\hbar}\, \mu_B B_0 , \tag{8}$$

the resonator natural frequency ω, and the anisotropy frequency

$$\omega_D = (2S-1)\frac{D}{\hbar} . \tag{9}$$

The resonance conditions

$$\left|\frac{\omega - \omega_0}{\omega_0}\right| \ll 1 , \qquad \frac{\omega_D}{\omega_0} \ll 1 \tag{10}$$

are assumed. For typical magnetic molecules, $\omega_D \sim (10^{10} - 10^{12})$ s^{-1}.

The most important relaxation parameters are the spin-phonon attenuation $\gamma_1 \equiv 1/T_1$, the spin-spin dephasing parameter $\gamma_2 \equiv 1/T_2$, and the resonator damping γ. For magnetic nanomolecules, the characteristic values are $\gamma_1 \sim (10^{-7} - 10^{-5})$ s^{-1} and $\gamma_2 \sim 10^{10}$ s^{-1}. Other attenuation mechanisms are discussed in Ref. [13].

The derivation of the equations of motion for the spin operators has been described in detail earlier [3,11,13]. Therefore, here we present the final form of these equations. To write down the equations in a compact way, we introduce the notations

$$\xi_i^0 \equiv \frac{1}{\hbar} \sum_{j(\neq i)} \left(a_{ij} S_j^z + c_{ij}^* S_j^- + c_{ij} S_j^+\right) ,$$

$$\xi_i \equiv \frac{i}{\hbar} \sum_{j(\neq i)} \left(2c_{ij} S_j^z - \frac{1}{2}\, a_{ij} S_j^- + 2b_{ij} S_j^+\right) , \tag{11}$$

in which $S_j^{\pm}$ are the ladder spin operators and the dipolar coefficients are

$$a_{ij} \equiv D_{ij}^{zz} \; , \qquad b_{ij} \equiv \frac{1}{4}\left(D_{ij}^{xx} - D_{ij}^{yy} - 2iD_{ij}^{xy} \right) \; , \qquad c_{ij} \equiv \frac{1}{2}\left(D_{ij}^{xx} - iD_{ij}^{yz} \right) \; . \tag{12}$$

Also, we define the effective force acting on the j spin as

$$f_j \equiv -\frac{i}{\hbar}\, \mu_0 H + \xi_j \; . \tag{13}$$

Taking into account the saturation effect [13,28], the effective transverse attenuation can be represented as

$$\Gamma_2 = \gamma_2 \left(1 - s^2 \right) \; , \tag{14}$$

in which

$$s \equiv \frac{1}{SN} \sum_{j=1}^{N} < S_j^z > \tag{15}$$

is the reduced longitudinal spin polarization. Using the above notations, we obtain [3,11,13] the equations of motion for the ladder spin operator $S_j^- \equiv S_j^x - iS_j^y$,

$$\frac{dS_j^-}{dt} = -i \left(\omega_0 + \xi_j^0 - i\Gamma_2 \right) S_j^- + f_j S_j^z + i\, \frac{\omega_D}{S}\, S_j^z S_j^- \; , \tag{16}$$

and for the component S_j^z,

$$\frac{dS_j^z}{dt} = -\frac{1}{2}\left(f_j^+ S_j^- + S_j^+ f_j \right) - \gamma_1 \left(S_j^z - \zeta \right) \; , \tag{17}$$

where ζ is an equilibrium spin polarization.

Our aim is to study the behaviour of the reduced spin polarization (15) as a function of time, $s = s(t)$, starting from a given initial polarization $s_0 \equiv s(0)$. The speed of the polarization reversal is connected with the level of the magnetodipole radiation characterized by the radiation intensity

$$I(t) = \frac{2\mu_0^2}{3c^3} \left| \sum_j < \ddot{\mathbf{S}}_j > \right|^2 \; , \tag{18}$$

where the overdots mean the time differentiation. In order to analyze to what extent the radiation is coherent, we separate in the radiation intensity (18), the coherent and incoherent parts,

$$I(t) = I_{inc}(t) + I_{coh}(t) \; , \tag{19}$$

with the incoherent and coherent radiation intensities

$$I_{inc}(t) \equiv \frac{2\mu_0^2}{3c^3} \sum_j \left| < \ddot{\mathbf{S}}_j > \right|^2 \; , \qquad I_{coh}(t) \equiv \frac{2\mu_0^2}{3c^3} \sum_{i \neq j} < \ddot{\mathbf{S}}_i \ddot{\mathbf{S}}_j > \; , \tag{20}$$

respectively.

We analyze the temporal evolution of $s(t)$ and $I(t)$ under different system parameters. Our final goal is to find the conditions providing the largest radiation intensity.

3 Results of calculations

We have investigated the equations of motion (16) and (17), with the equation (6) for the resonator feedback field, in two ways. First, the spins S_j^α have been treated as operator variables. Then, to find the behaviour of the spin polarization (15), we need to average the evolution equations (16) and (17). The following analysis is based on the scale separation approach [2,3,6–9], which is an extension of the averaging techniques [29] to the systems of stochastic differential equations. The second way of analyzing Eqs. (16) and (17) is by computer modeling, when S_j^α are treated as classical variables.

The first way, using the scale separation approach [2,3,6–9], better describes the initial stage of spin relaxation, when the coherence of spin motion has not yet been developed and quantum effects prevail. At this stage, the radiation intensity is very low, since the spins move chaotically. Such a chaotic stage lasts during the *chaos time* t_c, which can be estimated [13] as $t_c \sim (1 - s_0^2)/\omega_0 s_0$. For $s_0 = 0.9$ and $\omega_0 \sim 10^{13}$ s^{-1}, this gives $t_c \sim 10^{-14}$ s. After the time t_c, the dynamic coherence quickly develops, when the semiclassical approximation becomes applicable. At this coherent stage, the direct computer simulation gives a more appropriate description. The results of both methods of calculations, as we have checked, are close to each other, provided that in computer modeling one starts with $s_0 < 1$. The main difference is that the scale separation approach, being a kind of the averaging techniques, yields, for the solutions of the evolution equations their guiding centers, with fast oscillations being smoothed out. Since, at the coherent stage, the semiclassical approximation is well justified, we present below the results of direct numerical modeling, employing Eqs. (16) and (17), where spins are treated as classical variables.

In the figures below, time is measured in units of T_2 and all frequencies, in units of γ_2. We assume the resonance condition $\omega_0 = \omega$. The initial spin polarization in all figures, except Figs. 4 and 5, is taken as $s_0 = 0.9$. Other system parameters are listed in the related figure captions.

The radiation intensity is shown in reduced units, so that its maximum be close to one. In order to connect the calculated intensity with physical units, we measure our numerical results using the units of $N^2 I_0$, where N is the number of molecular spins and

$$I_0 \equiv \frac{2\mu_0^2}{3c^3}\,\gamma_2^4 \qquad (\mu_0 = -2\mu_B)$$

is a characteristic radiation intensity of a single spin. With $\mu_B = 0.9274 \times 10^{-20}$ erg/G, $\mu_0 = 1.855 \times 10^{-20}$ erg/G, and $\gamma_2 = 10^{10}$ s^{-1}, we have $I_0 = 0.852 \times 10^{-38}$ W, where 1W$= 10^7$ erg/s.

In Figs. 1 and 2, we study the influence of the Zeeman frequency ω_0 on the speed of polarization reversal and the level of radiation intensity. The fastest reversal and the strongest radiation occurs for the largest Zeeman frequency. Note that the present-day experimental facilities allow one to reach quite large values of magnetic field [30] and, consequently, to satisfy the inequality $\omega_0 \gg \omega_D$, which is necessary for achieving the resonance condition (10).

Figure 3 shows how the relaxation process depends on the value of the resonator damping γ. There exists an optimal value of γ, for which the final spin relaxation is kept fixed at the lowest level. However, for achieving the fastest reversal and the strongest radiation, the smallest γ is preferable.

The role of the initial spin polarization s_0 is demonstrated in Figs. 4 and 5. As is seen, the fastest polarization reversal and the strongest radiation intensity happens under the largest initial polarization.

Figures 6 and 7 show how the anisotropy frequency ω_D hinders the resonance condition (10). The larger ω_D, the stronger it suppresses the velocity of spin reversal and the maximal value of the radiation intensity.

Dipole interactions also suppress the relaxation process and the radiation intensity, as is seen in Figs. 8 and 9. The maximal intensity is diminished by the factor of 1.52. However, the dipole interactions are inavoidable in spin systems.

It is appropriate to recollect it again that dipole interactions do not allow for the realization of spin superradiance in resonatorless magnets [3,11–14,27]. Decoherent influence of dipole interactions can be overcome only by coupling the spin sample with a resonator producing sufficiently strong feedback field.

In addition to the necessary presence of a resonator, the role of dipole interactions can be regulated by varying the sample shape and orientation with respect to the external magnetic field and the direction of the resonator feedback field. This is illustrated in Figs. 10 and 11 which show that the best spin reversal and the strongest radiation intensity corresponds to the case of a spin chain directed along the axis of the resonant magnetic coil, that is, along the direction of the resonator feedback field.

To estimate the power of radiation intensity that can be obtained in real physical systems, we may accept for the number of coherently radiating molecules the coherence number

$$N_{coh} = \rho\lambda^3 \qquad \left(\lambda \equiv \frac{2\pi c}{\omega_0}\right) .$$

Taking the typical density of magnetic molecules in molecular magnets $\rho \approx 0.4 \times 10^{21}$ cm^{-3} and setting $\omega_0 = 2 \times 10^{13}$ s^{-1}, with $\lambda = 0.943 \times 10^{-2}$ cm, we get $N_{coh} \approx 10^{14}$. Then the maximal value of the radiation intensity (18) can be as high as $I_{max} \sim 10^5$ W. Comparing the incoherent and coherent parts of the intensity, as defined in Eq. (20), shows that the radiation in its maximum is practically completely coherent.

In conclusion, we have demonstrated that nanomolecues, as well as nanoclusters, can produce coherent spin radiation, provided they are coupled to a resonant electric circuit. Spin reversal can be made very fast, of the order of 10^{-11} s, which defines the duration of the coherent radiation pulse $t_p \sim 10^{-11}$ s. For magnetic nanomolecues, the maximal radiation intensity can reach 10^5 W. To achieve the strongest radiation requires to choose the largest ω_0 and s_0, but the smallest γ and ω_D. The sample shape and its orientation are important for obtaining the strongest radiation. The most favourable configuration corresponds to an elongated spin sample placed along the direction of the resonator feedback field.

Acknowledgement

Two of the authors (V.I.Y. and E.P.Y.) acknowledge financial support from the Russian Foundation for Basic Research (Grant 08-02-00118).

References

[1] N. Bloembergen and R.V. Pound, Phys. Rev. **95**, 8 (1954).

[2] V.I. Yukalov and E.P. Yukalova, Phys. Part. Nucl. **31**, 561 (2000).

[3] V.I. Yukalov and E.P. Yukalova, Phys. Part. Nucl. **35**, 348 (2004).

[4] V.I. Yukalov, Laser Phys. **2**, 559 (1992).

[5] T.S. Belozerova, V.K. Henner, and V.I. Yukalov, Phys. Rev. B **46**, 682 (1992).

[6] V.I. Yukalov, Phys. Rev. Lett. **75**, 3000 (1995).

[7] V.I. Yukalov, Laser Phys. **5**, 526 (1995).

[8] V.I. Yukalov, Laser Phys. **5**, 970 (1995).

[9] V.I. Yukalov, Phys. Rev. B **53**, 9232 (1996).

[10] V.I. Yukalov and E.P. Yukalova, Phys. Rev. Lett. **88**, 257601 (2002).

[11] V.I. Yukalov, Laser Phys. **12**, 1089 (2002).

[12] V.I. Yukalov and E.P. Yukalova, Europhys. Lett. **70**, 306 (2005).

[13] V.I. Yukalov, Phys. Rev. B **71**, 184432 (2005).

[14] V.I. Yukalov, V.K. Henner, and P.V. Kharebov, Phys. Rev. B **77**, 134427 (2008).

[15] B. Barbara, L. Thomas, F. Lionti, I. Chiorescu, and A. Sulpice, J. Magn. Magn. Mater. **200**, 167 (1999).

[16] A. Caneschi, D. Gatteschi, S. Sangregorio, R. Sessoli, L. Sorace, A. Cornia, M. Novak, C. Paulsen, and W. Wernsdorfer, J. Magn. Magn. Mater. **200**, 182 (1999).

[17] R.H. Kodama, J. Magn. Magn. Mater. **200**, 359 (1999).

[18] G.C. Hadjipanays, J. Magn. Magn. Mater. **200**, 373 (1999).

[19] A. Sukhov and J. Berakdar, arXiv:0802.1740 (2008).

[20] S. Ostanin, S.S. Razee, J.B. Staunton, B. Ginatempo, and E. Bruno, J. Appl. Phys. **93**, 453 (2003).

[21] C. Antoniak, J. Lindner, and M. Farle, Europhys. Lett. **70**, 250 (2005).

[22] C. Antoniak, J. Lindner, M. Spasova, D. Sudfeld, M. Acet, and M. Farle, Phys. Rev. Lett. **97**, 117201 (2006).

[23] I.D. Tokman, V.I. Pozdnjakova, G.A. Vugalter, and A.V. Shvetsov, Phys. Rev. B **77**, 094414 (2008).

[24] G.S. Agarwal, Springer Tracts Mod. Phys. **70**, 1 (1974).

[25] V.I. Yukalov, Laser Phys. Lett. **2**, 356 (2005).

[26] U.K. Kopvillem, V.R. Nagibarov, V.V. Samartsev, and N.K. Solovarov, Adv. Mol. Relax. Processes **8**, 241 (1976).

[27] V.I. Yukalov and E.P. Yukalova, Laser Phys. Lett. **2**, 302 (2005).

[28] A. Abraham and M. Goldman, Nuclear Magnetism: Order and Disorder (Clarendon, Oxford, 1982).

[29] N.N. Bogolubov and Y.A. Mitropolsky, Asymptotic Methods in the Theory of Nonlinear Oscillations (Gordon abd Breach, New York, 1961).

[30] M. Motokawa, Rep. Prog. Phys. **67**, 1995 (2004).

Figure Captions

Fig. 1. Reduced spin polarization $s(t)$ as a function of dimensionless time (measured in units of T_2) for a cubic sample of $N = 125$ molecules with spin $S = 10$. Initial reduced polarization is $s_0 = 0.9$, the anisotropy frequency is $\omega_D = 20$, and the resonator damping is $\gamma = 10$. The Zeeman frequency is varied: $\omega_0 = 1000$ (solid line), $\omega_0 = 2000$ (long-dashed line), and $\omega_0 = 5000$ (short-dashed line). The fastest polarization reversal is for the largest Zeeman frequency.

Fig. 2. Radiation intensity $I(t)$ for the parameters of Fig. 1 for different Zeeman frequencies: $\omega_0 = 1000$ (solid line), intensity is in units of 3.199×10^{13} N^2I_0; $\omega_0 = 2000$ (long-dashed line), intensity is in units of 0.832×10^{15} N^2I_0; $\omega_0 = 5000$ (short-dashed line), intensity is in units of 5.118×10^{16} N^2I_0. The strongest intensity is for the largest Zeeman frequency.

Fig. 3 Reduced spin polarization $s(t)$ as a function of dimensionless time for a cubic sample of N=125 molecules, with spin $S = 10$, initial polarization $s_0 = 0.9$, Zeeman frequency $\omega_0 = 2000$, and anisotropy frequency $\omega_D = 20$, for different resonator dampings: $\gamma = 1$ (solid line), $\gamma = 10$ (long-dashed line), and $\gamma = 50$ (short-dashed line). The fastest polarization reversal is for the smallest resonator damping, which yields the largest radiation intensity of order 10^{15} N^2I_0.

Fig. 4 Reduced spin polarization $s(t)$ as a function of dimensionless time for a cubic sample of $N = 125$ molecules, with spin $S = 10$, Zeeman frequency $\omega_0 = 2000$, anisotropy frequency $\omega_D = 20$, resonator damping $\gamma = 10$, for different initial polarizations: $s_0 = 0.9$ (solid line), $s_0 = 0.7$ (long-dashed line), and $s_0 = 0.5$ (short-dashed line). The fastest polarization reversal occurs for the largest initial polarization.

Fig. 5. Radiation intensity $I(t)$ for the parameters of Fig. 4 for varying initial polarizations: $s_0 = 0.9$ (solid line), $s_0 = 0.7$ (long-dashed line), and $s_0 = 0.5$ (short-dashed line). Intensity units are 0.832×10^{15} N^2I_0. The strongest radiation intensity is for the largest initial polarization.

Fig. 6. Reduced spin polarization $s(t)$ as a function of dimensionless time for a cubic sample of $N = 125$ molecules of spin $S = 10$, with the Zeeman frequency $\omega_0 = 2000$ and resonator damping $\gamma = 10$, for different magnetic anisotropy frequencies: $\omega_D = 20$ (solid line), $\omega_D = 50$ (long-dashed line), and $\omega_D = 100$ (short-dashed line). The fastest polarization reversal occurs for the smallest magnetic anisotropy.

Fig. 7. Radiation intensity $I(t)$ for the parameters of Fig. 6 for varying magnetic anisotropy frequencies: $\omega_D = 20$ (solid line), $\omega_D = 50$ (long-dashed line), and $\omega_D = 100$ (short-dashed line). The values of the radiation intensity are in units of 0.832×10^{15} N^2I_0. The strongest radiation intensity is for the weakest magnetic anisotropy.

Fig. 8. Reduced spin polarization $s(t)$ as a function of dimensionless time for a cubic sample of $N = 125$ molecules of spin $S = 10$, with $\omega_0 = 2000$, $\omega_D = 20$, and $\gamma = 10$, for the

case of present dipole interactions (solid line) and the case when they are absent (dashed line). The polarization reversal is hindered by dipole interactions.

Fig. 9. Radiation intensity $I(t)$ for the parameters of Fig. 8 for the cases with dipole interactions (solid line) and without these interactions (dashed line). Solid line corresponds to the intensity in units 0.806×10^{15} N^2I_0 and dashed line, in units 1.228×10^{15} N^2I_0. Radiation intensity is supressed by dipole interactions by the factor 1.524.

Fig. 10. Reduced spin polarization $s(t)$ as a function of dimensionless time for $N = 144$ molecules of spin $S = 10$, with $\omega_0 = 2000$, $\omega_D = 20$, and $\gamma = 30$, for different sample shapes and orientations: the chain of spins along the z-axis (solid line), the chain along the x-axis (long-dashed line), the $y - z$ plane of spins (short-dashed line), and the $x - y$ plane of spins (dotted-dashed line). The fastest and strongest spin reversal occurs for the case of the spin chain along the x-axis coinciding with the resonator axis.

Fig. 11. Radiation intensity $I(t)$ as a function of dimensionless time for $N = 144$ molecules of spin $S = 10$, with the same parameters as in Fig. 10, for different sample shapes and orientations: the spin chain along the z-axis (solid line), the spin chain along the x-axis (long-dashed line), the $y - z$ spin plane (short-dashed line), and the $x - y$ spin plane (dashed-dotted line). The strongest radiation intensity is for the spin chain along the x-axis, reaching in the maximum 1.206×10^{15} N^2I_0.

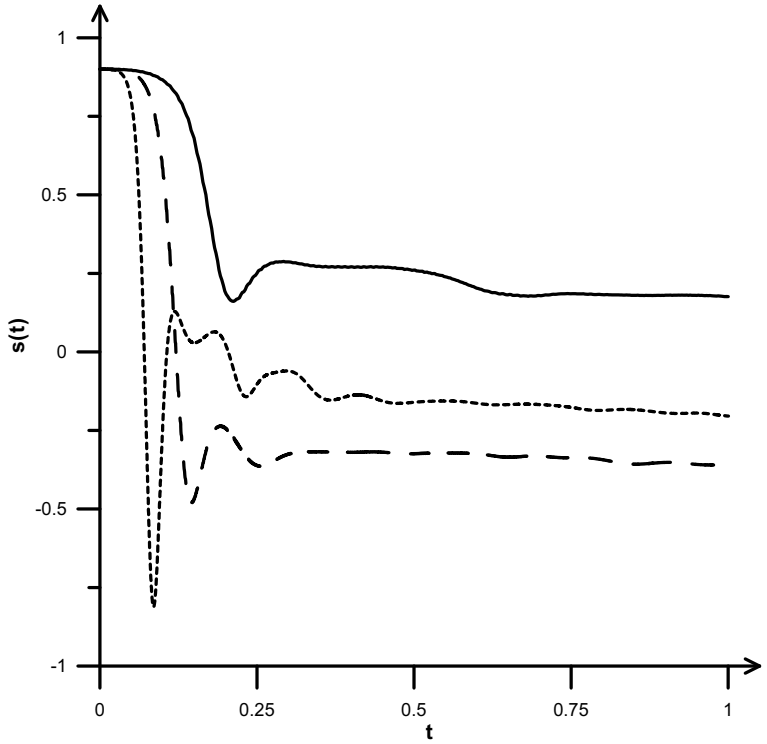

Figure 1: Reduced spin polarization $s(t)$ as a function of dimensionless time (measured in units of T_2) for a cubic sample of $N = 125$ molecules with spin $S = 10$. Initial reduced polarization is $s_0 = 0.9$, the anisotropy frequency is $\omega_D = 20$, and the resonator damping is $\gamma = 10$. The Zeeman frequency is varied: $\omega_0 = 1000$ (solid line), $\omega_0 = 2000$ (long-dashed line), and $\omega_0 = 5000$ (short-dashed line). The fastest polarization reversal is for the largest Zeeman frequency.

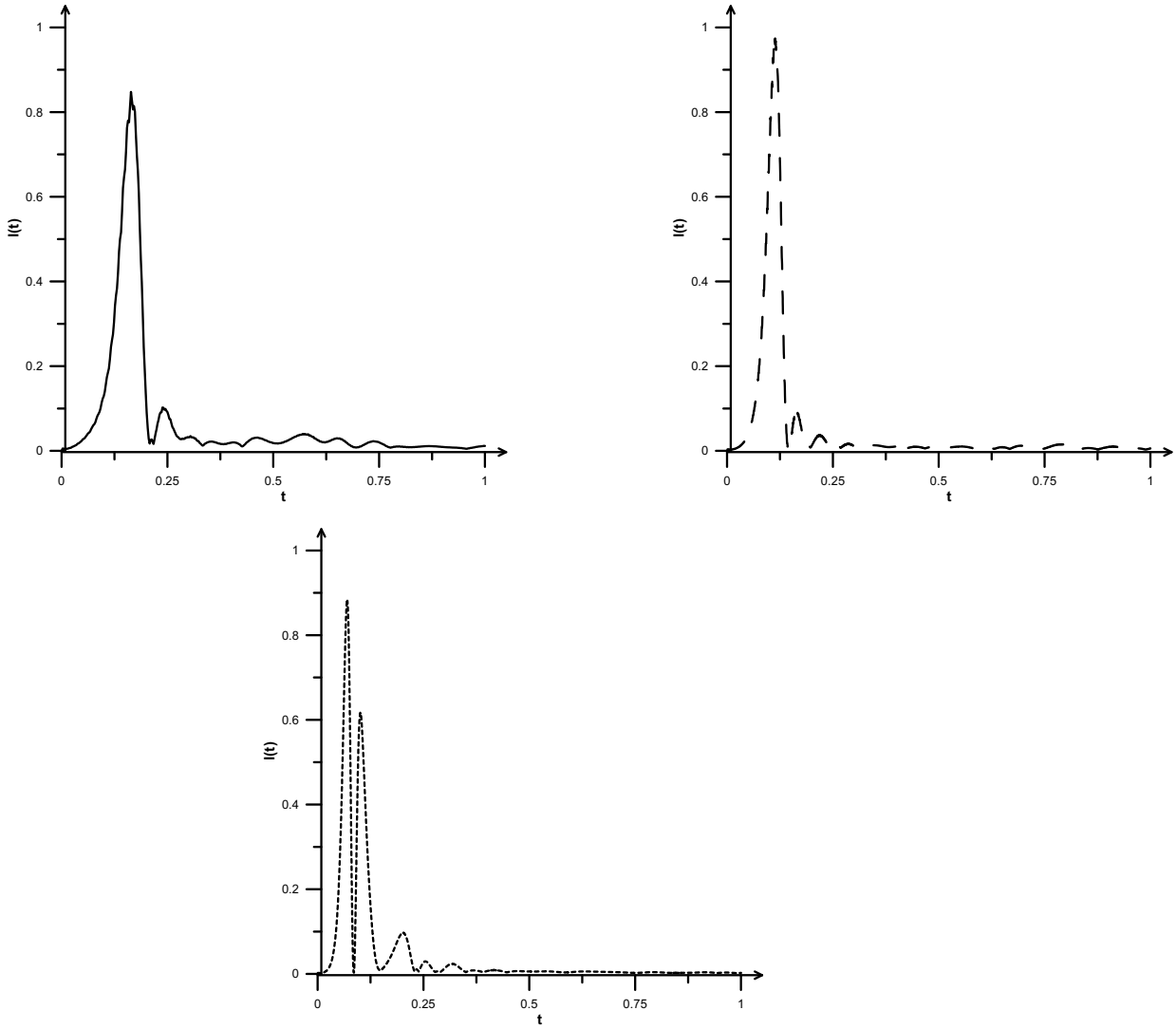

Figure 2: Radiation intensity $I(t)$ for the parameters of Fig. 1 for different Zeeman frequencies: $\omega_0 = 1000$ (solid line), intensity is in units of 3.199×10^{13} $\mathrm{N^2I_0}$; $\omega_0 = 2000$ (long-dashed line), intensity is in units of 0.832×10^{15} $\mathrm{N^2I_0}$; $\omega_0 = 5000$ (short-dashed line), intensity is in units of 5.118×10^{16} $\mathrm{N^2I_0}$. The strongest intensity is for the largest Zeeman frequency.

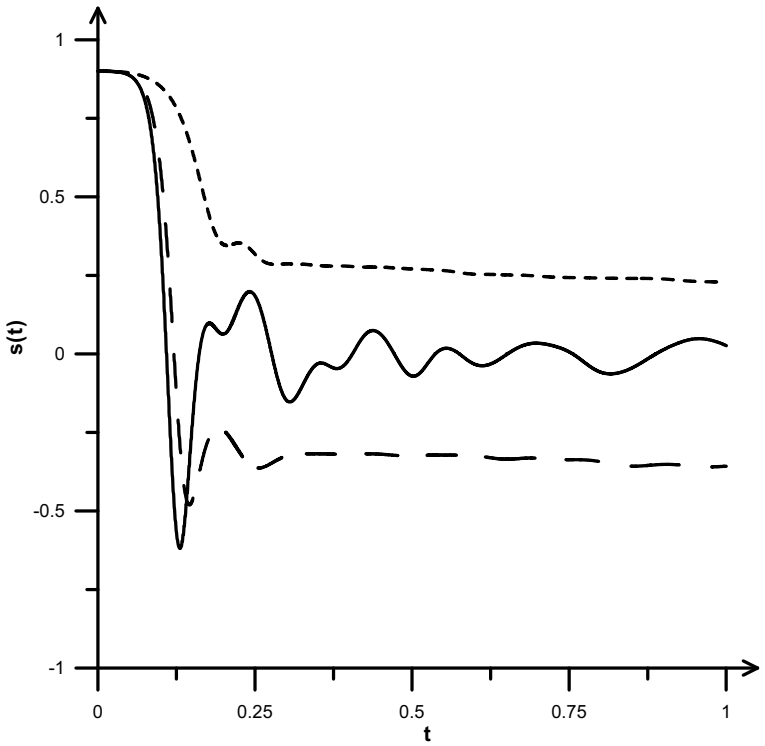

Figure 3: Reduced spin polarization $s(t)$ as a function of dimensionless time for a cubic sample of N=125 molecules, with spin $S = 10$, initial polarization $s_0 = 0.9$, Zeeman frequency $\omega_0 = 2000$, and anisotropy frequency $\omega_D = 20$, for different resonator dampings: $\gamma = 1$ (solid line), $\gamma = 10$ (long-dashed line), and $\gamma = 50$ (short-dashed line). The fastest polarization reversal is for the smallest resonator damping, which yields the largest radiation intensity of order 10^{15} $N^2 I_0$.

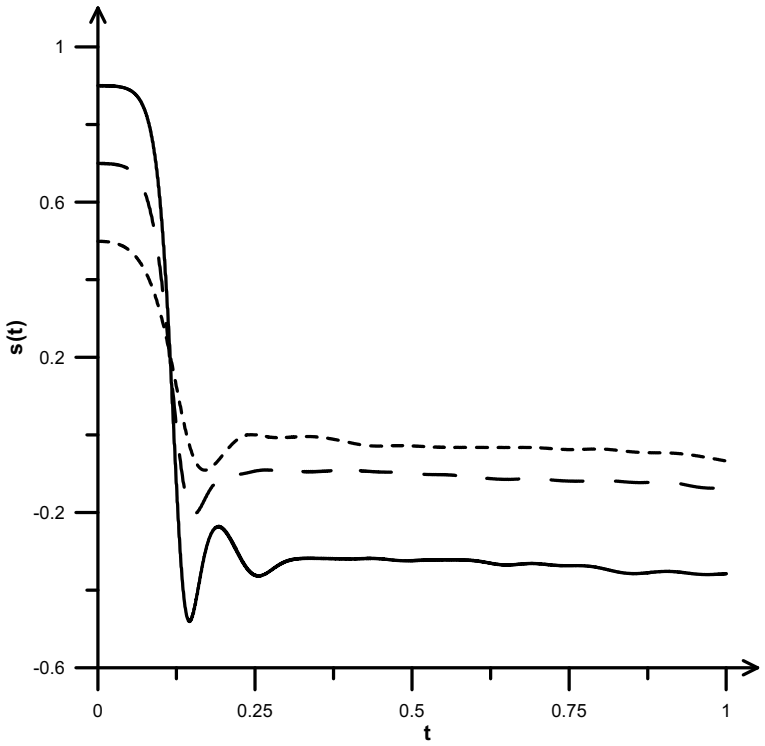

Figure 4: Reduced spin polarization $s(t)$ as a function of dimensionless time for a cubic sample of $N = 125$ molecules, with spin $S = 10$, Zeeman frequency $\omega_0 = 2000$, anisotropy frequency $\omega_D = 20$, resonator damping $\gamma = 10$, for different initial polarizations: $s_0 = 0.9$ (solid line), $s_0 = 0.7$ (long-dashed line), and $s_0 = 0.5$ (short-dashed line). The fastest polarization reversal occurs for the largest initial polarization.

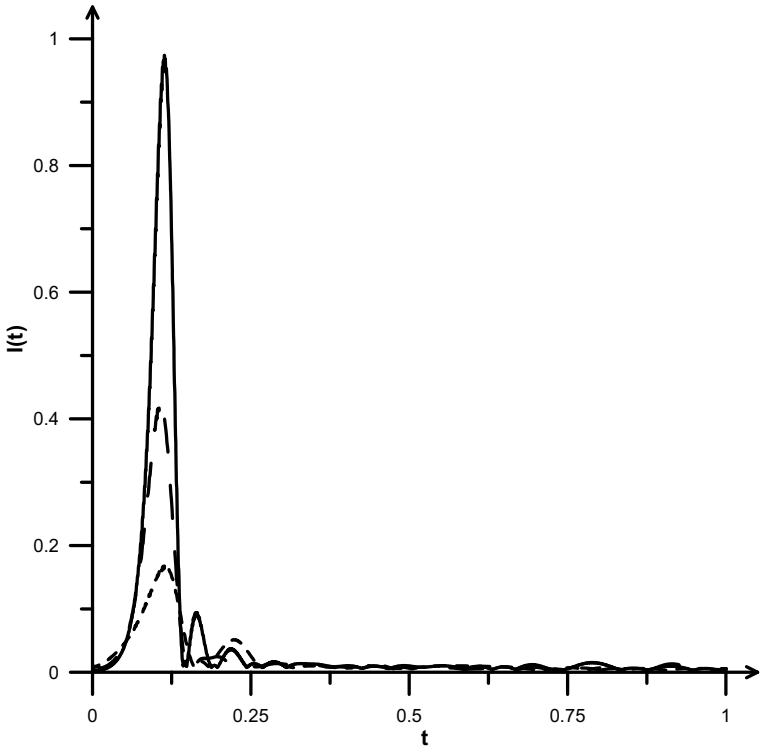

Figure 5: Radiation intensity $I(t)$ for the parameters of Fig. 4 for varying initial polarizations: $s_0 = 0.9$ (solid line), $s_0 = 0.7$ (long-dashed line), and $s_0 = 0.5$ (short-dashed line). Intensity units are 0.832×10^{15} $\mathrm{N^2I_0}$. The strongest radiation intensity is for the largest initial polarization.

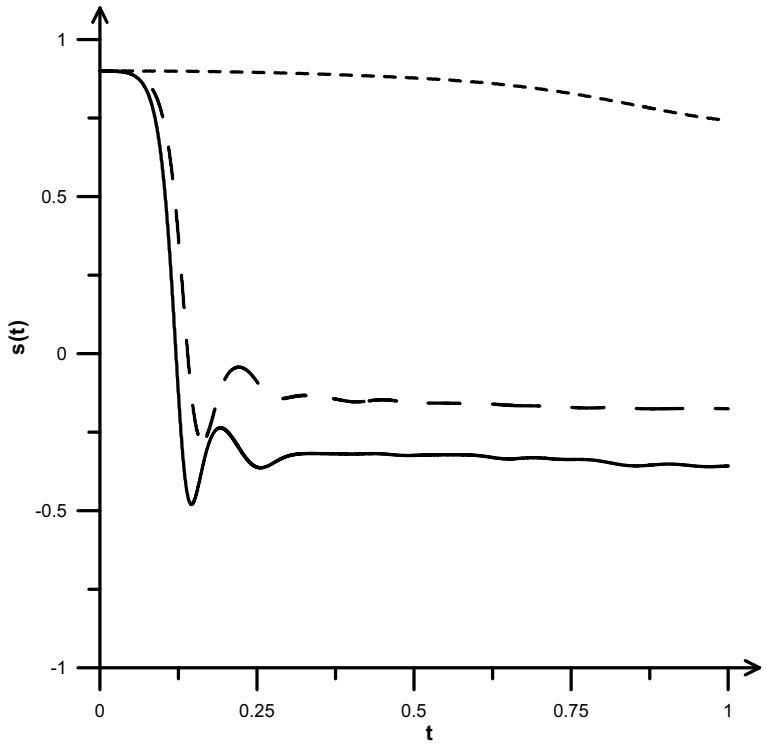

Figure 6: Reduced spin polarization $s(t)$ as a function of dimensionless time for a cubic sample of $N = 125$ molecules of spin $S = 10$, with the Zeeman frequency $\omega_0 = 2000$ and resonator damping $\gamma = 10$, for different magnetic anisotropy frequencies: $\omega_D = 20$ (solid line), $\omega_D = 50$ (long-dashed line), and $\omega_D = 100$ (short-dashed line). The fastest polarization reversal occurs for the smallest magnetic anisotropy.

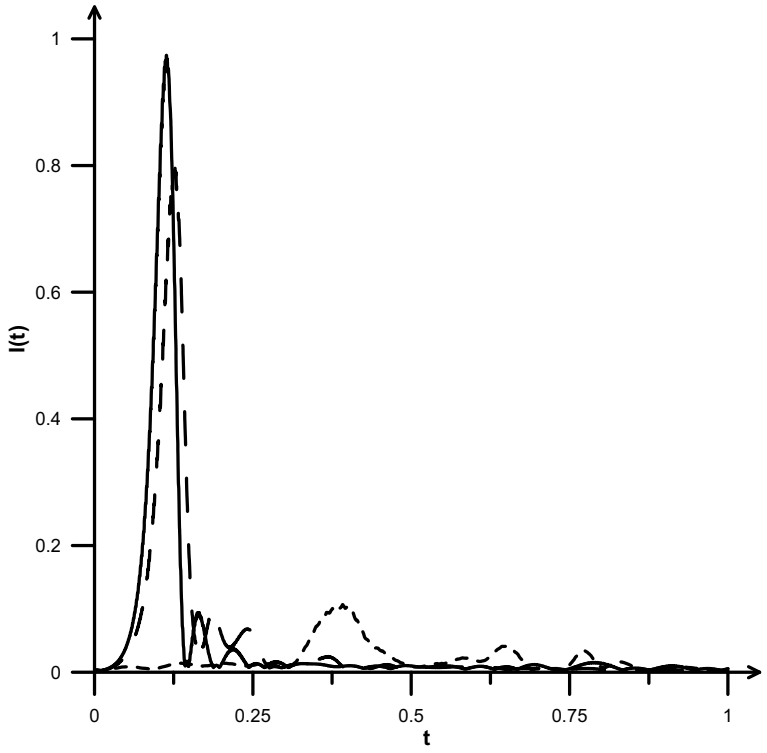

Figure 7: Radiation intensity $I(t)$ for the parameters of Fig. 6 for varying magnetic anisotropy frequencies: $\omega_D = 20$ (solid line), $\omega_D = 50$ (long-dashed line), and $\omega_D = 100$ (short-dashed line). The values of the radiation intensity are in units of 0.832×10^{15} $N^2 I_0$. The strongest radiation intensity is for the weakest magnetic anisotropy.

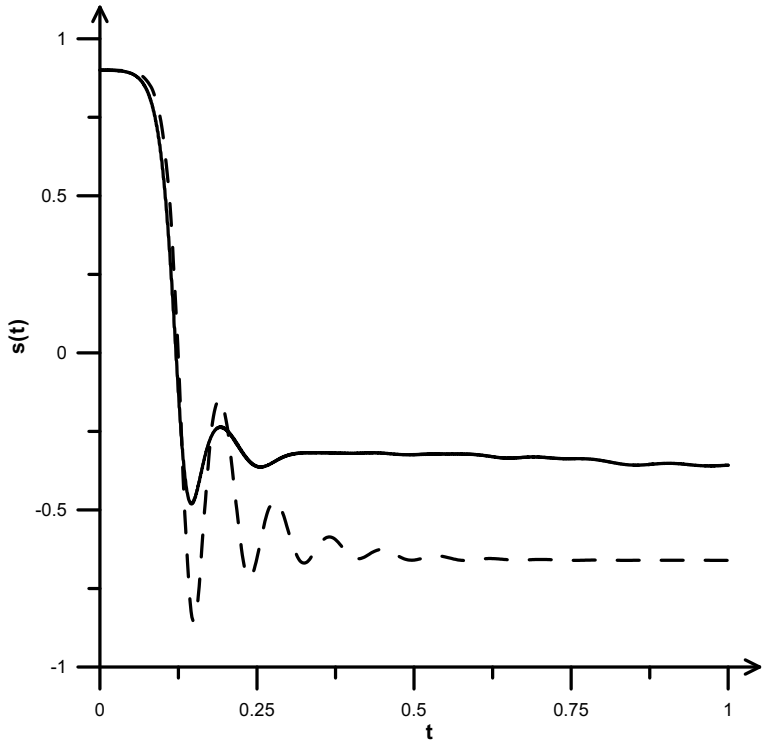

Figure 8: Reduced spin polarization $s(t)$ as a function of dimensionless time for a cubic sample of $N = 125$ molecules of spin $S = 10$, with $\omega_0 = 2000$, $\omega_D = 20$, and $\gamma = 10$, for the case of present dipole interactions (solid line) and the case when they are absent (dashed line). The polarization reversal is hindered by dipole interactions.

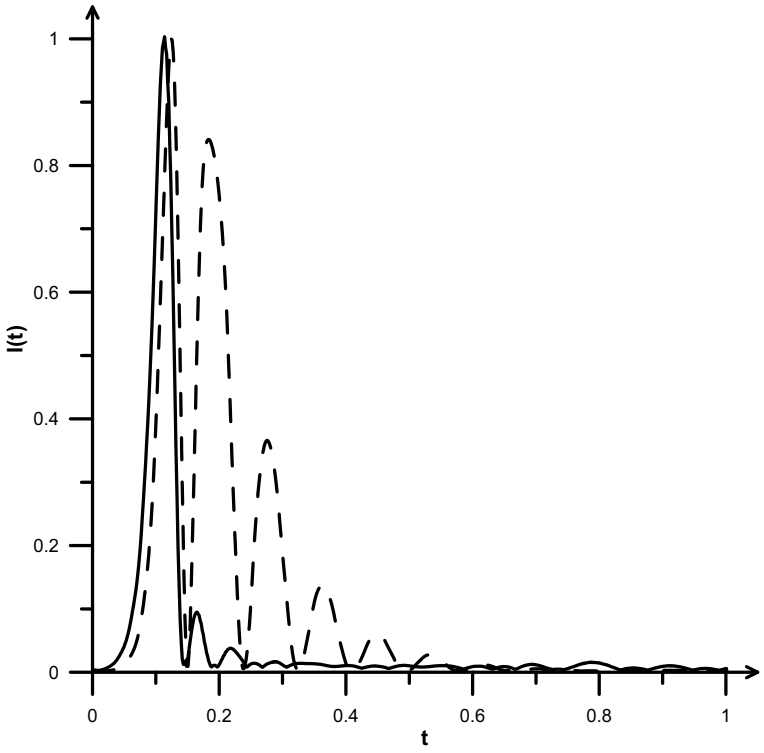

Figure 9: Radiation intensity $I(t)$ for the parameters of Fig. 8 for the cases with dipole interactions (solid line) and without these interactions (dashed line). Solid line corresponds to the intensity in units 0.806×10^{15} N^2I_0 and dashed line, in units 1.228×10^{15} N^2I_0. Radiation intensity is supressed by dipole interactions by the factor 1.524.

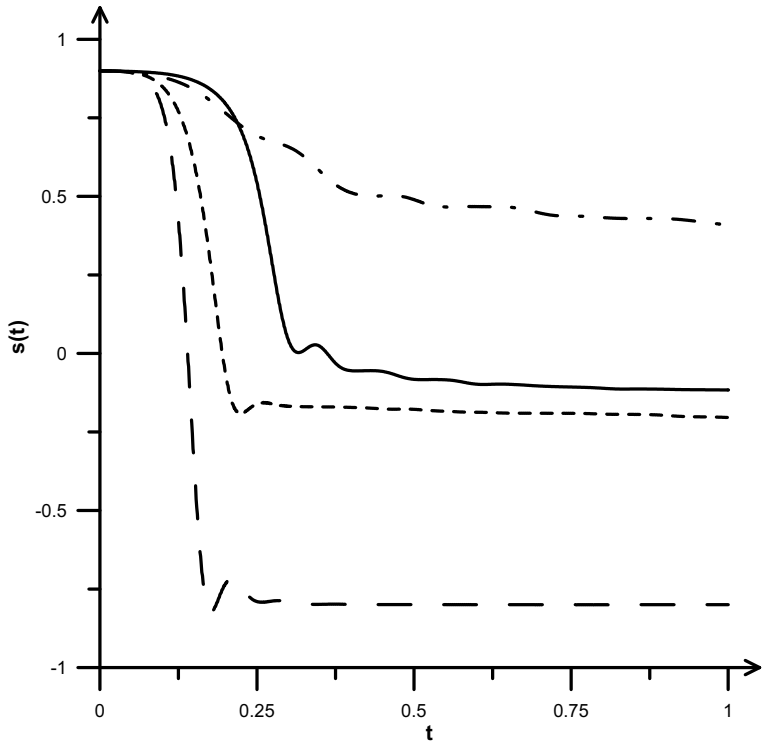

Figure 10: Reduced spin polarization $s(t)$ as a function of dimensionless time for $N = 144$ molecules of spin $S = 10$, with $\omega_0 = 2000$, $\omega_D = 20$, and $\gamma = 30$, for different sample shapes and orientations: the chain of spins along the z-axis (solid line), the chain along the x-axis (long-dashed line), the $y - z$ plane of spins (short-dashed line), and the $x - y$ plane of spins (dotted-dashed line). The fastest and strongest spin reversal occurs for the case of the spin chain along the x-axis coinciding with the resonator axis.

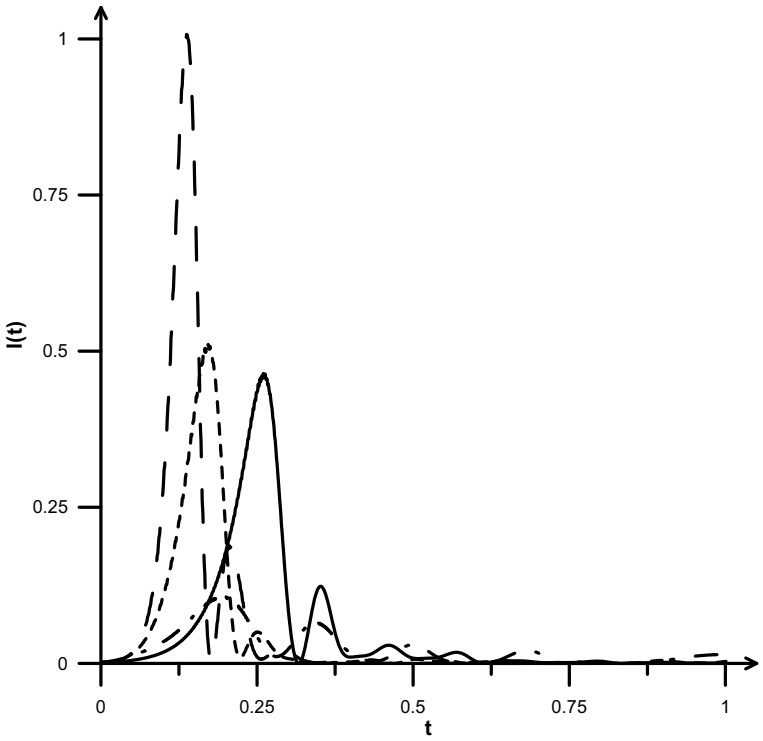

Figure 11: Radiation intensity $I(t)$ as a function of dimensionless time for $N = 144$ molecules of spin $S = 10$, with the same parameters as in Fig. 10, for different sample shapes and orientations: the spin chain along the z-axis (solid line), the spin chain along the x-axis (long-dashed line), the $y-z$ spin plane (short-dashed line), and the $x-y$ spin plane (dashed-dotted line). The strongest radiation intensity is for the spin chain along the x-axis, reaching in the maximum 1.206×10^{15} $\mathrm{N^2 I_0}$.